HHS Public Access

Author manuscript

Acta Biomater. Author manuscript; available in PMC 2022 January 08.

Published in final edited form as:

Acta Biomater. 2021 December ; 136: 233–242. doi:10.1016/j.actbio.2021.09.041.

Evaluation of a self-fitting, shape memory polymer scaffold in a rabbit calvarial defect model

Michaela R. Pfau[a], **Felipe O. Beltran**[b], **Lindsay N. Woodard**[a], **Lauren K. Dobson**[d], **Shelby B. Gasson**[d], **Andrew B. Robbins**[e], **Zachary T. Lawson**[a], **W. Brian Saunders**[d], **Michael R. Moreno**[a,e], **Melissa A. Grunlan**[a,b,c,*]

[a]Department of Biomedical Engineering, Texas A&M University, College Station, Texas 77843, US

[b]Department of Materials Science and Engineering, Texas A&M University, College Station, Texas 77843, US

[c]Department of Chemistry, Texas A&M University, College Station, Texas 77843, US

[d]Department of Small Animal Clinical Sciences, Texas A&M University, College Station, Texas 77843, US

[e]Department of Mechanical Engineering, Texas A&M University, College Station, Texas 77843, US

Abstract

Self-fitting scaffolds prepared from biodegradable poly(ε-caprolactone)-diacrylate (PCL-DA) have been developed for the treatment of craniomaxillofacial (CMF) bone defects. As a thermoresponsive shape memory polymer (SMP), with the mere exposure to warm saline, these porous scaffolds achieve a conformal fit in defects. This behavior was expected to be advantageous to osseointegration and thus bone healing. Herein, for an initial assessment of their regenerative potential, a pilot *in vivo* study was performed using a rabbit calvarial defect model. Exogenous growth factors and cells were excluded from the scaffolds. Key scaffold material properties were confirmed to be maintained following gamma sterilization. To assess scaffold integration and neotissue infiltration along the defect perimeter, non-critically sized (d = 8 mm) bilateral calvarial defects were created in 12 New Zealand white rabbits. Bone formation was assessed at 4 and 16 weeks using histological analysis and micro-CT, comparing defects treated with an SMP scaffold (d = 9 mm x t = 1 or 2 mm) to untreated defects (i.e. defects able to heal without intervention). To further assess osseointegration, push-out tests were performed at 16 weeks and compared to defects treated with poly(ether ether ketone) (PEEK) discs (d = 8.5 mm x t = 2 mm). The results of this study confirmed that the SMP scaffolds were biocompatible and highly conducive to bone formation and ingrowth at the perimeter. Ultimately, this resulted in similar bone volume and surface area versus untreated defects and superior performance in push-out testing versus defects treated with PEEK discs.

*Corresponding author. mgrunlan@tamu.edu (M.A. Grunlan).

Declaration of Competing Interest

The authors declare that they have no competing interest.

Supplementary materials

Supplementary material associated with this article can be found, in the online version, at doi:10.1016/j.actbio.2021.09.041.

Keywords

Calvarial defect; Shape memory polymer (SMP) scaffolds; Tissue engineering; Rabbit; Biomechanics

1. Introduction

Confined, craniomaxillofacial (CMF) bone defects arise from a variety of clinical scenarios, including trauma, tumor resection, congenital deformities, surgical burr holes, and craniotomy [1]. Annually in the USA, ~10 million CMF trauma cases occur [2], including >400,000 facial fractures [3]. Significant incidence rates have prompted a global CMF device market valued at 1.6 billion USD in 2020, predicted to grow 9% annually [4]. Over 6% of the total 1.6 M bone grafts implanted annually were craniofacial bone grafts [5]. Indeed, autografting remains the “gold standard” of treatment despite numerous drawbacks, including surgical harvesting, donor site morbidity, and limited availability [6–10]. However, CMF defects frequently exhibit irregular geometries, such that rigid autografts are difficult to shape and position within the defect, often resulting in insufficient bone-to-graft contact leading to poor osseointegration and possible graft resorption [11–13].

The limitations of autografting have prompted alternative approaches, particularly those based on biomaterials that can achieve a conformal fit [7,8,14,15]. Capable of i*n situ* cure, bone cements and putties that are typically comprised of poly(methyl methacrylate) (PMMA) and a bioactive glass or glass ceramic filler, emerged in the 1940s [16–20]. These are limited by their slow setting times, brittle nature (leading to post-surgical fracture), exothermic cures as high as 90 °C (leading to tissue necrosis), and post-cure shrinkage (resulting in diminished tissue contact) [21–23]. While advances have been made to improve their porosity and degradability [24–26], tissue regeneration is generally limited with cements and putties. Patient-specific implants (PSIs) have more recently been developed, wherein an implant matching the defect geometry is created by preoperative processing of a patient’s CT-scans, computer-aided design (CAD) of a virtual implant, and 3D printing of the actual implant [27–31]. Polyetheretherketone (PEEK) is most often utilized, favored due to its similar mechanical properties to bone tissue (e.g. modulus and yield strength). However, in addition to the time intensive process to prepare PEEK CMF PSIs, the lack of porosity at the perimeter limits integration with adjacent bone. While recent reports have described 3D printed PEEK with macroporosity with potential for improved osseointegration [32,33], PSIs prepared as such would likewise be limited by an exhaustive preparation process and the lack of degradability to permit complete tissue regeneration.

Tissue engineering (TE) is a promising alternative to treat CMF bone defects [34,35]. The scaffold plays an essential role to the success of this approach and must exhibit key properties, including: (1) conformal fit within the defect to permit osseointegration, (2) biodegradability and interconnected pores for osteoconduction, and (3) mechanical robustness to prevent collapse or brittle fracture. To address this unmet need in CMF bone regeneration, we have reported “self-fitting” shape memory polymer (SMP) scaffolds based on biodegradable poly(*ε*-caprolactone)-diacrylate (PCL-DA) [36,37]. The crystalline

lamellae (T_m or "T_{trans}" ~55 °C) serve as the switching segments, and the crosslinks form the netpoints. Thus, the porous SMP scaffold becomes malleable when exposed to warm saline or air (T ~55 °C) due to the lamellae melting. This allows the scaffolds to be press-fitted into regular- or irregularly-shaped defects, wherein shape recovery promotes scaffold expansion to the perimeter. With cooling ($T < T_{trans}$), the lamellae recrystallize and the scaffold undergoes shape fixity, locking it in its new shape within the defect. In addition to the conformal fit and perimeter contact (for osseointegration) afforded by the scaffold's shape memory behavior, several other beneficial properties were also realized. Fabrication using solvent-casting particulate leaching (SCPL) with a fused salt template produced scaffolds with pores sizes associated with osteogenesis (~220 μm); [38] high porosity (~70%) and interconnectivity for cellular and neotissue infiltration were also achieved. The scaffolds were mechanically robust, and lacked brittleness, withstanding 85% strain without fracture [39]. PCL-DA SMP scaffolds were shown to be non-cytotoxic and to support the adhesion and proliferation of human osteoblasts [37]. Upon coating the scaffolds with a bioactive polydopamine coating, there was approximately a 5-fold increase in cellular adhesion and proliferation as well a 1.6-fold increase in expression of runX2. The polydopamine-coated scaffolds also formed deposits of hydroxyapatite (HAp) upon exposure to simulated body fluid (SBF, 1X). In subsequent studies, we demonstrated that the PCL-DA scaffolds could be fabricated with an incorporated cell adhesion peptide (NH_2-Arg-Gly-Asp-Ser-COOH; RGD) [40]. When seeded with bone marrow-derived human mesenchymal stem cells (h-MSCs) and cultured in the absence of osteogenic supplements, polydopamine-coated and RGD-containing scaffolds improved osteogenesis relative to uncoated scaffolds.

In this work, a pilot *in vivo* study was performed using a rabbit calvarial defect model for a preliminary assessment of the healing potential of "self-fitting" PCL-DA scaffolds (Fig. 1). To evaluate the inherent bone healing capacity of the scaffold, a cell adhesive peptide and polydopamine coating were both excluded. Furthermore, exogenous cells and growth factors were also not included. In this way, the scaffold represents a biologic-free and bioactive coating-free, off-the-shelf surgical product. The scaffolds were subjected to gamma irradiation sterilization prior to implantation, and so, key properties of the scaffold were assessed before and after. A rabbit calvarial defect model is well-established in the literature [14,41]. Bilateral calvarial defects (d = 8 mm) were created in New Zealand white rabbits. While not critically sized, this scenario enabled the assessment of scaffold osseointegration and neotissue infiltration along the defect perimeter. This also reduced the number of animals utilized as two bilateral defects could be produced, rather than one central, critical-size defect (d = 15 mm), thus demonstrating a commitment to the 3R's principle of humane animal research [42,43]. Twelve rabbits were divided into three treatment groups (4 per group, N = 8 defects per group) with the prior group completed before beginning the next treatment group. Group I rabbits each received a SMP scaffold (d = 9 mm x t = 1 mm) [right] and an untreated defect [left]; these were terminated at 4 weeks. Group II rabbits each received a slightly thicker SMP scaffold (d = 9 mm x t = 2 mm) [right] and an untreated defect [left]; these were also terminated at 4 weeks. Group III rabbits (N = 2 rabbits, N = 4 defects) each received a SMP scaffold (d = 9 mm x t = 2 mm) [right] and an untreated defect [left]; these were terminated at 16 weeks. These specimens harvested from

Groups I-III were subjected to micro-CT and histological analysis. The remaining Group III rabbits (N = 2 rabbits, N = 4 defects) each received a SMP scaffold (d = 9 mm x t = 2 mm) [right] and a PEEK disc (d = 8.5 mm x t = 2 mm) [left]. The PEEK disc represented an established biomaterial implant with precedence in treating CMF defects. The diameter was selected to provide good contact and an interference fit with the adjacent tissue. This group was also terminated at 16 weeks, but was subjected to push-out tests using a custom biomechanical testing system.

2. Materials and methods

2.1. Materials

PCL-diol (M_n = 10k g/mol per manufacturer specifications), 4-(dimethylamino)pyridine (DMAP), triethylamine (Et_3N), acryloyl chloride, potassium carbonate (K_2CO_3), anhydrous magnesium sulfate ($MgSO_4$), sodium chloride (NaCl, salt) 2,2-dimethoxy-2-phenyl acetophenone (DMP), 1-vinyl-2-pyrrolidinone (NVP), dichloromethane (DCM), and other solvents were purchased from Sigma-Aldrich. All solvents were dried over 4 Å molecular sieves prior to use and all reagents were vacuum dried overnight prior to use. Salt was sieved using an ASTM E-11 no.40 sieve with 425 μm openings; scanning electron microscopy (SEM) and ImageJ showed an average salt size of 460 ± 70 μm. PEEK discs (d = 8.5 mm x t = 2 mm) used for push-out tests were prepared from PEEK blocks (source: KLS Martin) that were milled to the desired thickness and then cut to the targeted diameter with a CNC. Prior to implantation, PEEK discs were EtO-sterilized (Anderson Anprolene Sterilization Cabinet, AN-74i).

2.2. Scaffold fabrication

PCL-diacrylate (PCL-DA) was prepared per an established protocol [44]. PCL-DA scaffolds (Fig. 1b) were prepared using a SCPL protocol (Fig. 1c) as previously reported [37,45]. Briefly, a fused salt template was formed from 10.0 g of sieved salt and 7.5 wt% DI water within a 20 mL glass vial (I.D. = 25 mm) that was sequentially mechanically stirred, centrifuged (3220 x g, 15 min), and dried under vacuum (30 in. Hg, room temperature [RT], overnight [ON]). A PCL-DA solution (0.15 g per mL of DCM) was combined with a 15 vol% photoinitiator solution (10 wt% DMAP in NVP). The vortexed macromer solution (~5 mL) was added to the fused salt template, and centrifuged (1260 x g, 10 min) to promote solution diffusion throughout the template. Next, the vial exposed to UV-light (UV-Transilluminator, 6 mW cm^{-2} , 365 nm, 5 min) to cure the PCL-DA. Following solvent evaporation at RT ON, the cylindrical specimen was removed from the vial, and the salt template leached by soaking in water/ethanol (1:1 vol:vol) for 4 days with daily solution changes. Following air-drying (RT, 12 h), the specimen was annealed (30 in. Hg, 85 °C, 1 h). The resulting porous scaffold cylinders were then sliced (t = 1 or 2 mm) using a vibratome and were finally biopsy punched to a diameter of 9 mm (Fig. S1).

2.3. Scaffold characterization

Scaffold specimens (d = 9 mm x t = 1 mm) were evaluated having previously been subjected to gamma irradiation sterilization (KLS Martin, Germany), and compared to analogous non-sterilized specimens. Pore size was examined via scanning electron microscopy (SEM,

accelerating voltage ~10 kV, Au-Pt coating ~7 nm) and resultant images ($N = 4$) were analyzed (ImageJ). Pores on the diagonal midline were measured to obtain average pore diameter or average pore size. Scaffold specimen% porosity ($N = 3$) was calculated gravimetrically per Eq. (1), where the density of the analogous solid film ($N = 3$) is 1.19 g/mL:

$$Porosity\ (\%) = \frac{\rho_{solid\ film} - \rho_{porous\ scaf\ fold}}{\rho_{solid\ film}} * 100 \quad (1)$$

The $T_{m,PCL}$ (i.e. T_{trans}) and PCL% crystallinity of the scaffolds was determined by differential scanning calorimetry (DSC, TA Instruments Q100). Scaffold specimens (~10 mg; $N = 3$) were sealed in hermetic pans that were heated from RT to 80 °C at a rate of 5 °C/min. Values were taken from the first cycle. TA Universal Analysis software was used to determine the $T_{m,PCL}$ onset, and $T_{m,PCL}$ midpoint from the onset and the maximum of the endothermic melt peak, respectively. PCL% crystallinity was determined with Eq. (2), where the enthalpy of fusion (ΔH_m) is the area of the endothermic melt peak, the enthalpy of crystallization for the exothermic cold crystallization peak (ΔH_c), and the theoretical value for 100% crystalline PCL (ΔH°_m) is 139.5 J/g [46].

$$\%\chi_c = \frac{\Delta\ H_m - \Delta\ H_c}{\Delta\ H^\circ_m} * 100 \quad (2)$$

Compression tests were performed on scaffold specimens ($N = 3$, $d = 9$ mm x $t = 1$ mm) with an Instron 5944 at RT. Specimens were subjected to a constant strain (1.5 mm/min) up to 85% strain. Due to their non-brittle nature, fracture did not occur. From the resulting stress versus strain curves, the compressive modulus (E) was determined from the slope of the initial linear region (≤ 10% strain). The compressive strength (CS) was determined from the stress at 85% strain. The E of PEEK discs ($d = 8.5$ mm x $t = 2$ mm) were similarly determined.

2.4. Implantation

This study was approved by the Texas A&M University IACUC (AUP 2015–0240/2018–0403). Six-month-old New Zealand White rabbits ($N = 4$ rabbits per treatment group) were anesthetized using 40 mg/kg ketamine, 5 mg/kg xylazine, and 0.05 mg/kg acepromazine administered intramuscularly. Following induction, 0.12 mg/kg buprenorphine sustained release (Simbadol™ Zoetis) and 2 mg/kg carprofen (Rimadyl® Zoetis) were administered subcutaneously for analgesia. Additionally, 5 mL/kg Lactated Ringer's solution was administered subcutaneously. A surgical plane of anesthesia was maintained via isoflurane mask inhalation (1–3%, to effect). The hair coat of the dorsal aspect of the skull was clipped and removed and then aseptically prepared using alternating scrubs of 7.5% betadine and sterile saline solutions.

A 4 cm skin incision was created along the midline of the skull. The periosteum was carefully incised and elevated and retracted with Gelpi retractors. Bilateral full-thickness

calvarial defects were created in the parietal bones with an 8.0 mm diameter trephine burr (Ace Surgical Supply, Brockton, MA) under saline irrigation, with one defect positioned on either side of midline. To ensure proper placement, defects were created 1 to 2 mm from the sagittal and coronal sutures in all rabbits. The defects were either untreated, treated with a scaffold, or treated with a PEEK disc (Fig. 1a). For Groups I and II as well as designated Group III animals, the scaffolds were implanted into right calvarial defects, and left calvarial defects served as untreated defect controls. For Groups III animals reserved for biomechanical testing, the scaffolds were likewise implanted into right calvarial defects, and left calvarial defects were each treated with a PEEK disc. For scaffold implantation, individual specimens were placed in a sterile 55 °C saline bath for 30–60 s during defect drilling. The scaffolds were then assessed manually to ensure a malleable state, followed by brief wicking of warm saline and placement into each defect. In some instances, scaffolds were adjusted within the defect using sterile cotton tip applicators until they cooled and locked into position. Neither the surgical site or defects were irrigated or lavaged with 55 °C saline. The surgical site was lavaged with 37 °C saline prior to routine closure of deep tissues with 3–0 Monocryl in a simple continuous patterns. Skin was closed in a single layer using 4–0 Monocryl in an intradermal pattern. Group I and II rabbits were terminated at 4 weeks, and Group III rabbits were terminated at 16 weeks. At termination, rabbits were first sedated using ketamine, xylazine, and acepromazine as described above, followed by euthanasia with 100 mg/kg pentobarbital sodium (Euthasol® Virbac, Carros, France). Decapitation was performed postmortem, and skulls were submerged in 10% neutral buffered formalin at a minimum of 1:10 tissue to formalin ratio.

2.5. Gross examination, micro-CT, and histology

Gross dissection, histology, and micro-CT was performed on a fee-for-service basis by the Cardiovascular Pathology (CVP) Laboratory at Texas A&M University. Prior to manipulation, calvaria were assessed via micro-CT (NSI X50 micro-CT; North Star Imaging, Rogers, MN). Calvarial defects and adjacent healthy calvaria were excised using a Mopec Stryker Saw (Oak Park, MI). Calvarial samples were decalcified in Formical-4 solution (Fisher Scientific) and processed for histological evaluation by routine 5 μm thick sections and H&E or Masson's trichrome stains. Calvaria were assessed using qualitative and quantitative observations by a board-certified veterinary pathologist at the CVP.

2.6. Quantification of bone volume and surface area

Upon completion of micro-CT, quantification of bone formation was performed using. Mimics 20.0 (materialise, Plymouth, MI). Untreated control defects were used to optimize reconstruction parameters, and Hounsfield units (HU) were set between 24,518–34,952 HU for all reconstructions. New bone formation within the surgical defect was quantified by first generating a digital cylinder (d = 8 mm) within each defect. Tissue within each cylinder was thresholded using 24,518–34,952 HU to quantify bone volume (mm^3) and bone surface area (mm^2).

2.7. Biomechanical push-out testing

At 16 weeks, rabbits (N = 2) were terminated and calvaria were removed using a dremel diamond wheel and wrapped in an isotonic saline or 0.9% saline-soaked gauze sponges,

placed in specimen bags, and placed in a −20 °C freezer until testing. Push-out tests were performed with a custom biomechanical testing system that affords a comparative evaluation of shear stress (Fig. 2, Fig. S2) [47]. The push-out method was designed to meet four design objectives: (i) rigidly fix calvarial samples, (ii) minimize lateral bending, (iii) position the defect accurately, and (iv) permit verification of the coaxial alignment of the defect with the push-out rod. The core component of our design is a custom 3D printed hinged clamp with a 9.5 mm through-hole that circumferentially clamps the calvarial sample, constraining sample deformation. This clamp was affixed around the defect on the sample and centered under a flat-bottomed stainless steel push-out rod (d = 7.5 mm) that was attached to the end of the linear actuator on the custom biomechanical testing system. Displacement was zeroed at 5 N compressive preload then advanced at a rate of 5 mm/min (0.0083 mm/s) [48]. Force and displacement were measured with 100 lbf (444 N) load cell and 2 inch stroke linear variable differential transformer (LVDT), respectively. Failure load (N) and stiffness (N/mm) were calculated from the resulting load-extension curve. Stiffness (i.e., resistance to push-out force) was defined as the slope of the linear regression obtained from the most linear portion of the load-extension curve.

2.8. Statistical analysis

For scaffold material characterization before and after sterilization, data were reported as the mean ± standard deviation. Values were compared using Student's t-test and a p-value of <0.05 was considered statistically significant. Quantified bone volume and surface area were reported as mean ± standard deviation. Bone healing data between untreated control defects and PCL-DA implants were analyzed within each group using GraphPad Prism using two-way ANOVA with Sidak's multiple comparisons post-hoc test. Significance was established at $p < 0.05$. For the biomechanical push-out test, both load to failure and stiffness were assessed using a Students paired t-test and difference of means (μ) was reported; a p-value of <0.05 was considered statistically significant.

3. Results and discussion

3.1. SMP scaffold characterization

The scaffold specimens were prepared with a diameter (d = 9 mm) that was slightly larger than that of the calvarial defect (d = 8 mm, Fig. S3a). This was intentional in order to achieve circumferential scaffold contact with the defect perimeter during press-fitting. Prior to implantation into rabbit calvarial defects, scaffolds were sterilized via gamma irradiation. Thus, scaffold properties were assessed prior to sterilization and following sterilization (Table 1). Sterilization did not impact pore features; porosity (~70%) and average pore size (~220 μm) was maintained. PCL crystallinity is essential to shape memory behavior and thus to self-fitting capabilities, as well as to scaffold mechanical properties. DSC thermograms did not show any impact from sterilization (Fig. S4). Furthermore, the scaffold $T_{m,PCL}$ (i.e. T_{trans}) was determined to be ~52 °C ($T_{m,\ onset}$) and ~58 °C ($T_{m,\ midpoint}$), irrespective of prior sterilization. PCL% crystallinity was likewise not significantly changed (~60%). The robust mechanical properties of the scaffolds were also maintained with E ~20 MPa, and CS (at 85% strain) ~26 MPa. Owing to the retention of PCL% crystallinity, the ability of

scaffolds to be press-fitted into a model calvarial defect (d = 8 mm) was demonstrated (Fig. S3b).

3.2. Implantation

Sterilized scaffolds (d = 9 mm x t = 1 or 2 mm) were successfully implanted into bilateral calvarial defects (d = 8 mm) of New Zealand white rabbits (Fig. 1a, Fig. 3). To afford self-fitting, the scaffold specimens were exposed to warm saline near the T_{trans} (T ~55 °C) for 30–60 s prior to implantation. The malleable scaffolds were able to be gently pressed within the defects. There, the scaffold underwent shape recovery towards returning to its original shape and dimensions, expanding to the perimeter. The slightly larger original diameter of the scaffold further promoted good tissue contact. As the scaffold temperature cooled (T < 55 °C), it reverted to its relatively rigid state and so became shape fixed within the defect. From a surgical perspective, the scaffolds exhibited exceptional handling properties and press-fitting was readily achieved in all cases. Performed first, the Group I rabbits revealed important details on desired scaffold thickness. Based on literature values of rabbit calvaria, scaffold specimens were prepared with a thickness of 1 mm. However, when the defects were created, the excised tissue was observed to be nearly 2 mm thick (Fig. 4a). Upon implantation of these scaffolds (t = 1 mm), some slight buckling was observed. This was subsequently shown in a model defect, although contact with the perimeter was achieved (Fig. S5). Thus, for subsequent Groups II and III, scaffold thickness was increased to 2 mm (Fig. 5a). Upon press-fitting, these scaffolds did not exhibit any buckling as likewise shown with a model defect (Fig. S5). In the case of PEEK implants (d = 8.5 mm x t = 2 mm), the selected diameter provided the intended good tissue contact and an interference fit (Fig. S6). Because of their rigidity, greater pressure was required to insert PEEK discs into the defects versus the SMP scaffolds.

3.3. Gross examination and histology

Gross examination of Group I specimens (N = 4; 4 weeks) showed no appreciable differences in cerebral tissue for the defects treated with SMP scaffolds (compared to the untreated defect control (Fig. 4b). Histology revealed an expected amount of woven bone formation circumferentially around the defect controls, due to the non-critical defect size (Fig. 4c). Scaffolds contained islands of woven bone circumferentially around each implant.

For Group II (N = 4; 4 weeks), the increased scaffold thickness better paralleled the calvarial thickness (Fig. 5a). Gross examination revealed that, similar to Group I, no appreciable differences in cerebral tissue for the defects treated with scaffolds compared to untreated defects (Fig. 5b). Histology showed coalescing islands of eosinophilic to amphiphilic woven bone and complete bridging by new woven bone (Fig. 5c). For Group II defects treated with scaffolds, bone healing primarily occurred in the form of woven bone at the periphery of each scaffold, but a majority of the tissue intercalating and replacing the scaffold was non-ossified fibrous connective tissue. Red blood cells, implant detritus, and their clearing by phagocytic cells were also evident. This response is consistent with the expected healing response at 4 weeks. Notably, the implementation of thicker scaffolds improved the positioning of scaffolds and the ability to adequately fill the defect as evident in their lack of bowing.

For Group III ($N = 2$; 16 weeks), gross examination revealed expected smooth, regular contours for the untreated defect sites (Fig. 6a). In contrast, the defects treated with the SMP scaffolds showed evidence of a tan colored material, identified likely as the persisting SMP scaffold, bulging on the ventral surface. This slight bulging may be attributed to the manner in the scaffold (d ~ 9 mm) must occupy a somewhat smaller defect (d ~ 8 mm). In one animal, tan bone discoloration in surrounding tissue was observed. Histology (H&E staining) revealed that the SMP scaffolds were biocompatible (i.e., did not exhibit any long-term evidence of a protracted inflammatory response) (Fig. 6bc). Additionally, the defects treated with SMP scaffolds exhibited tissue ingrowth, both of blood vessels and fibrous tissue, with modest evidence of bone ingrowth into pores, particularly near the periphery at the site of bone-scaffold contact. These areas were characterized by an orderly layer of woven bone with typical marrow spaces, covered by variable amounts of orderly skeletal muscle, adipose tissue, and fibrous connective tissue. Trichrome staining further confirmed a modest amount of collagen within the sites treated with the scaffolds (Fig. 6d). While these findings were promising, there was a lack of bone in the center of the implant, likely impeded by PCL's slow degradation. Collectively, these results suggest that the SMP scaffolds were biocompatible at 4 and 16 weeks, and that bone growth was present within scaffold pores, particularly at the scaffold/defect interface.

3.4. Micro-CT analysis

Bone growth present in the scaffold pores and within the untreated defects of Groups I, II, and III was quantified by micro-CT (Fig. 7a) using generated 3D reconstructions (Fig. 7b). At 16 weeks, bone growth was markedly more substantial versus at 4 weeks. More bone was qualitatively apparent in the center of untreated defects versus within the central portion of the SMP scaffolds, expected in this non-critically sized defect model. However, when assessed quantitatively, there was no detectible difference in terms of the overall bone volume or surface area (Fig. 8, Table S1, Table S2). The explanation for these results is that while defects treated with SMPs did not have large amounts of bone within the center of the defects/SMPs, there was robust bone formation, osseointegration, and bone on-growth at the margins of the defects. These results suggest that the SMP scaffolds led to similar amounts of bone healing as compared to untreated defects (i.e., the scaffolds did not inhibit bone healing), with bone deposited more robustly at the interface between the SMPs and defects. These results are consistent with the histologic findings of new bone formation, particularly at the periphery of the SMP scaffolds. This is expected to promote scaffold osseointegration and stability, as assessed using push-out testing as described below.

3.5. Biomechanical push-out testing

For the other two animals from Group III, the scaffolds were likewise implanted into right calvarial defects, and left calvarial defects were each treated with a PEEK disc. Push-out tests were performed at 16 weeks. The pre-implantation modulus of the PEEK implants ($E = 220 \pm 19.0$ MPa) was orders of magnitude higher than that of the SMP scaffold (E ~20 MPa). Yet, the partially healed defects treated with SMP scaffolds were noticeably more resistant to pushout than the contralateral PEEK implants in terms of both the maximum load required (Fig. 9a) and stiffness (Fig. 9b). This is attributed to the favorable bone tissue ingrowth at the scaffold/defect perimeter, as observed histologically and by micro-CT.

Differences in failure load and stiffness were calculated for each rabbit as the value of the SMP scaffold treatment minus the value of the PEEK treatment (Table S3 and Table S4). A Students paired *t*-test performed on both the failure load ($\mu = 85.7$, $\sigma = 2.90$, $p = 0.0152$) and the stiffness ($\mu = 85.3$, $\sigma = 5.94$, $p = 0.0313$) showed the measured differences to be statistically significant. The porous SMP scaffolds likely surpassed the solid PEEK controls biomechanically due to tissue ingrowth especially at the perimeter, consistent with histological and micro-CT findings. Moreover, these findings support the notion that the self-fitting SMP scaffold offer clinical advantages for treatment of CMF defects due to improved osseointegration.

4. Conclusion

The healing potential of a “self-fitting” scaffold was assessed in a pilot study utilizing a rabbit calvarial defect model. Based on biodegradable PCL, the porous scaffold’s shape memory nature uniquely affords press-fitting and conformability into defects. Devoid of exogeneous growth factors or bioactive coatings, the scaffold is reliant on the unique mechanism to achieve good contact with the defect perimeter as well as pore interconnectivity to achieve osseointegration. Prior to implantation, scaffolds were sterilized with gamma irradiation and shown to retain key material properties. The study was design to assess initial bone ingrowth and infiltration at the scaffold/defect interface and the resulting osseointegration. Thus, a non-critical size defect model was employed, wherein the untreated defect control would undergo healing. In general, the SMP scaffolds were shown to support woven bone formation particularly at the scaffold periphery, and to support bone ingrowth comparable to the untreated control, determined via microCT at 4 and 16 weeks of healing. At 16 weeks, the SMP scaffold outperformed implanted PEEK discs when assessed via push out-test tests. While PEEK is much more rigid, the scaffold supported superior osseointegration and thus greater implant biomechanical stability. Collectively, these results support the potential of SMP scaffolds to treat CMF bone defects. Future work will assess its performance in larger defects and/or other models towards an off-the-shelf regenerative CMF device.

Supplementary Material

Refer to Web version on PubMed Central for supplementary material.

Acknowledgement

This work was supported in part by KLS Martin. Funding from NIH NIDCR 1R01DE025886-01A1 and the NSF Graduate Research Fellowship Program (NSF GRFP) (L.W.) is gratefully acknowledged.

References

[1]. Haug RH, Morgan JP, Etiology, distribution, and classification of traumatic craniomaxillofacial deformities and defects, in: Greenberg AM, Schmelzeisen R (Eds.), Craniomaxillofacial Reconstructive and Corrective Bone Surgery, Springer New York, New York, NY, 2019, pp. 45–51,

[2]. Moses H , Powers D , Keeler J, Erdman D , Marcus J , Puscas L , Woodard C, Opportunity cost of surgical management of craniomaxillofacial trauma, Craniomaxillofac. Trauma Reconstr. 9 (2016) 76–81,

[3]. Allareddy V , Allareddy V , Nalliah RP , Epidemiology of facial fracture injuries, J. Oral Maxillofac. Surg 69 (10) (2011) 2613–2618, [PubMed: 21683499]

[4]. Craniomaxillofacial Devices Market Size, Share & Trends Analysis Report By Material (Metal, Ceramics), By Product (CMF Plate & Screw Fixation, Bone Graft Substitute), By Application, And Segment Forecasts, 2021 - 2028, pp. 1–128.

[5]. Greenwald AS, Boden SD, Goldberg VM, Khan Y, Laurencin CT, Rosier RN, Bone-graft substitutes: facts, fictions, and applications, J. Bone Jt. Surg. Am 83 (2001) 98–103,

[6]. Elsalanty ME , Genecov DG , Bone grafts in craniofacial surgery, Craniomaxillofac. Trauma Reconstr 2 (2009) 125–134, [PubMed: 22110806]

[7]. Neovius E , Engstrand T, Craniofacial reconstruction with bone and biomaterials: review over the last 11 years, J. Plast. Reconstr. Aesthet. Surg 63 (10) (2010) 1615–1623. [PubMed: 19577527]

[8]. Song T , Qiu Z-Y , Qui F-Z , Biomaterials for reconstruction of cranial defects, Front. Mater. Sci 9 (2015) 346–354.

[9]. Betz RR, Lavelle WF, Samdani AF, Bone grafting options in children, Spine (Phila Pa 1976) 35 (17) (2010) 1648–1654. [PubMed: 20628337]

[10]. Tessier P, Kawamoto H, Matthews D, Posnick J, Raulo Y, Tulasne JF, Wolfe SA, Autogenous bone grafts and bone substitutes—Tools and techniques: I. A 20,000-case experience in maxillofacial and craniofacial surgery, Plast. Reconstr. Surg 116 (5) (2005) 6S–24S . [PubMed: 16217441]

[11]. Lee SH , Yoo CJ , Lee U , Park CW, Lee SG , Kim WK , Resorption of autogenous bone graft in cranioplasty: resorption and reintegration failure, Korean J. Neurotrauma 10 (2014) 10–14. [PubMed: 27169026]

[12]. Moreira-Gonzalez ITAJ, Miyawaki T, Barakat K, DiNick V, Clinical outcome in cranioplasty: critical review in longterm follow-up, J. Craniofac. Surg 14 (2003) 144–153. [PubMed: 12621283]

[13]. Grant GA , Jolley M , Ellenbogen RG , Roberts TS , Gruss JR , Loeser JD, Failure of autologous bone—Assisted cranioplasty following decompressive craniectomy in children and adolescents, J. Neurosurg. Pediatrics 100 (2004) 163–168 .

[14]. Szpalski C, Barr J, Wetterau M, Saadeh PB, Warren SM , Cranial bone defects: current and future strategies, Neurosurg. Focus 29 (6) (2010) E8.

[15]. Pryor LS, Gage E, Langevin C-J, Herrera F, Breithaupt AD, Gordon CR, Afifi AM, Zins JE, Meltzer H, Gosman A, Cohen SR, Holmes R, Review of bone substitutes, Craniomaxillofac. Trauma Reconstr. 2 (3) (2009) 151–160.

[16]. Arora M, Chan EK, Gupta S, Diwan AD, Polymethylmethacrylate bone cements and additives: a review of the literature, World J. Orthop 4 (2013) 67–74. [PubMed: 23610754]

[17]. Kenny SM, Buggy M, Bone cements and fillers: a review, J. Mater. Sci. Mater. Med 14 (2003) 923–938. [PubMed: 15348504]

[18]. Magnan B, Bondi M, Maluta T, Samaila E, Schirru L, Dall'Oca C, Acrylic bone cement: current concept review, Musculoskelet. Surg 97 (2) (2013) 93–100.

[19]. Low KL, Tan SH, Zein SHS, Roether JA, Mouriño V, Boccaccini AR, Calcium phosphate-based composites as injectable bone substitute materials, J. Biomed. Mater. Res. Part B 94 (1) (2010) 273–286.

[20]. Giannoudis PV , Dinopoulos H, Tsiridis E, Bone substitutes: an update, Injury 36S (2005) S20–S27.

[21]. Abdulghani S, Mitchell GR , Biomaterials for in situ tissue regeneration: a review, Biomolecules 9 (2019) 750.

[22]. Dias JR , Ribeiro N , Baptista-Silva S , Costa-Pinto AR , Alves N , Oliveira AL, *In situ* enabling approaches for tissue regeneration: current challenges and new developments, Front. Bioeng. Biotechnol 8 (2020) 85. [PubMed: 32133354]

[23]. Orr JF, Dunne NJ, Quinn JC , Shrinkage stresses in bone cement, Biomaterials 24 (17) (2003) 2933–2940. [PubMed: 12742733]

[24]. Dall'Oca C, Maluta T, Cavani F, Morbioli GP , Bernard P, Sbarbat A, Degl'Innocenti D, Magnan B, The biocompatibility of porous vs non-porous bone cements: a new methodological approach, Eur. J. Histochem 58 (2) (2014) 2255 . [PubMed: 24998920]

[25]. Henslee AM, Gwak D-H, Mikos AG , Kasper FK, Development of a biodegradable bone cement for craniofacial applications, J. Biomed. Mater. Res. A 100A (9) (2012) 2252–2259.

[26]. Domb AJ, Manor N, Elmalak O, Biodegradable bone cement compositions based on acrylate and epoxide terminated poly(propylene fumarate) oligomers and calcium salt compositions, Biomaterials 17 (4) (1996) 411–417, [PubMed: 8938235]

[27]. Rammos CK, Cayci C, Castro-Garcia JA, Feiz-Erfan I, Lettieri SC, Patient-specific polyetheretherketone implants for repair of craniofacial defects, J. Craniofac. Surg 26 (3) (2015) 631–633, [PubMed: 25901667]

[28]. Zegers T, ter Laak-Poort M, Koper D, Lethaus B, Kessler P, The therapeutic effect of patient-specific implants in cranioplasty, J. Craniomaxillofac. Surg 45 (1) (2017) 82–86. [PubMed: 27916400]

[29]. Alonso-Rodriguez E , Cebrián JL, Nieto MJ, Del Castillo JL, Hernández-Godoy J, Burgueño M, Polyetheretherketone custom-made implants for craniofacial defects: report of 14 cases and review of the literature, J. Craniomaxillofac. Surg 43 (7) (2015) 1232–1238 . [PubMed: 26032759]

[30]. Bonda DJ, Manjila S, Selman WR, Dean D, The recent revolution in the design and manufacture of cranial implants: modern advancements and future directions, Neurosurgery 77 (5) (2015) 814–824. [PubMed: 26171578]

[31]. Guevara-Rojas G, Figl M, Schicho K, Seemann R, Traxler H, Vacariu A, Carbon C-C, Ewers R, Watzinger F, Patient-specific polyetheretherketone facial implants in a computer-aided planning workflow, J. Oral Maxillofac. Surg 72 (9) (2014) 1801–1812. [PubMed: 24679957]

[32]. Elhattab K, Sikder P, Walker JM, Bottino MC , Bhaduri SB, Fabrication and evaluation of 3-D printed PEEK scaffolds containing macropores by design, Mater. Lett 263 (2020) 127227.

[33]. Spece H , Yu T , Law AW, Marcolongo M , Kurtz SM , 3D printed porous PEEK created via fused filament fabrication for osteoconductive orthopaedic surfaces, J. Mech. Beh. Biomed. Mater 109 (2020) 103850.

[34]. Alsberg E, Hill EE, Mooney DJ, Craniofacial tissue engineering, Crit. Rev. Oral Biol. Med 12 (2001) 64–75. [PubMed: 11349963]

[35]. Petrovic V, Zivkovic P, Petrovic D, Stefanovi V , Craniofacial bone tissue engineering, Oral Surg. Oral Med. Oral Pathol, Oral Radiol 114 (3) (2012),

[36]. Grunlan MA, Zhang D, Schoener CA, Saunders WB, US 9925297: Shape memory Polymer Scaffolds For Tissue Defects, The Texas A&M University System, College Station, TX, USA, 2018 3 27.

[37]. Zhang D, George OJ, Petersen KM, Jimenez-Vergara AC, Hahn MS, Grunlan MA , A bioactive "self-fitting" shape memory polymer scaffold with potential to treat cranio-maxillo facial bone defects, Acta Biomater 10 (11) (2014) 4597–4605. [PubMed: 25063999]

[38]. Bružauskaitė I, Bironaitė D, Bagdonas E, Bernotienė E, Scaffolds and cells for tissue regeneration: different scaffold pore sizes different cell effects, Cytotechnology 68 (2016) 355–369. [PubMed: 26091616]

[39]. Beltran FO, Houk CJ, Grunlan MA, Bioactive siloxane-containing shape-memory polymer (SMP) scaffolds with tunable degradation rates, ACS Biomater. Sci. Eng (2021) in press, online.

[40]. Erndt-Marino JD , Munoz-Pinto DJ, Samavedi S, Jimenez-Vergara AC, Diaz-Rodriguez P, Woodard L, Zhang D, Grunlan MA, Hahn MS, Evaluation of the osteoinductive capacity of polydopamine-coated poly(ϵ-caprolactone) diacrylate shape memory foams, ACS Biomater. Sci. Eng 1 (12) (2015) 1220–1230. [PubMed: 33304994]

[41]. Liu N , Lyu X , Fan H , Shi J , Hu J , Luo E , Animal models for craniofacial reconstruction by stem/stromal cells, Curr. Stem Cell Res. Ther 9 (2014) 174–186. [PubMed: 24524796]

[42]. Russell WM , The development of the three Rs concept, Altern Lab Anim 23 (3) (1995) 298–304, [PubMed: 11656565]

[43]. Zurlo J, Rudacille D, Goldberg AM, The three Rs: the way forward, Environ. Health Perspect 104 (8) (1996) 878–880. [PubMed: 8875163]

[44]. Woodard LN, Page VM , Kmetz KT, Grunlan MA , PCL-PLLA semi-IPN shape memory polymers (SMPs): degradation and mechanical properties, Macromol. Rapid Comm 37 (2016) 1972–1977.

[45]. Pfau MR, McKiney KG, Roth AA, Graul LM, Maitland DJ, Grunlan MA, Shape memory polymer (SMP) scaffolds with improved self-fitting properties, J. Mater. Chem. Part B (2021) in press online.

[46]. Woodard LN, Kmetz KT , Roth AA , Page VM, Grunlan MA, Porous poly(ε-caprolactone)–poly(L-lactic acid) semi-interpenetrating networks as superior, defect-specific scaffolds with potential for cranial bone defect repair, Biomacromolecules 18 (12) (2017) 4075–4083. [PubMed: 29037044]

[47]. Lawson ZTH, Saunders J-W, Grunlan WB, A. M; Moreno MR; Robbins AB, Methodology for performing biomechanical push-out tests for evaluating the osseointegration of calvarial defect repair in small animal models, in review.

[48]. Spicer PP, Kretlow JD, Young S, Jansen JA, Kasper FK, Mikos AG , Evaluation of bone regeneration using the rat critical size calvarial defect, Nat. Protoc 7 (10) (2012) 1918–1929. [PubMed: 23018195]

Statement of significance

Current treatments of craniomaxillofacial (CMF) bone defects include biologic and synthetic grafts but they are limited in their ability to form good contact with adjacent tissue. A regenerative engineering approach using a biologic-free scaffold able to achieve conformal fitting represents a potential “off-the-shelf” surgical product to heal CMF bone defects. Having not yet been evaluated *in vivo*, this study provided the preliminary assessment of the bone healing potential of self-fitting PCL scaffolds using a rabbit calvarial defect model. The study was designed to assess scaffold biocompatibility as well as bone formation and ingrowth using histology, micro-CT, and biomechanical push-out tests. The favorable results provide a basis to pursue establishing self-fitting scaffolds as a treatment option for CMF defects.

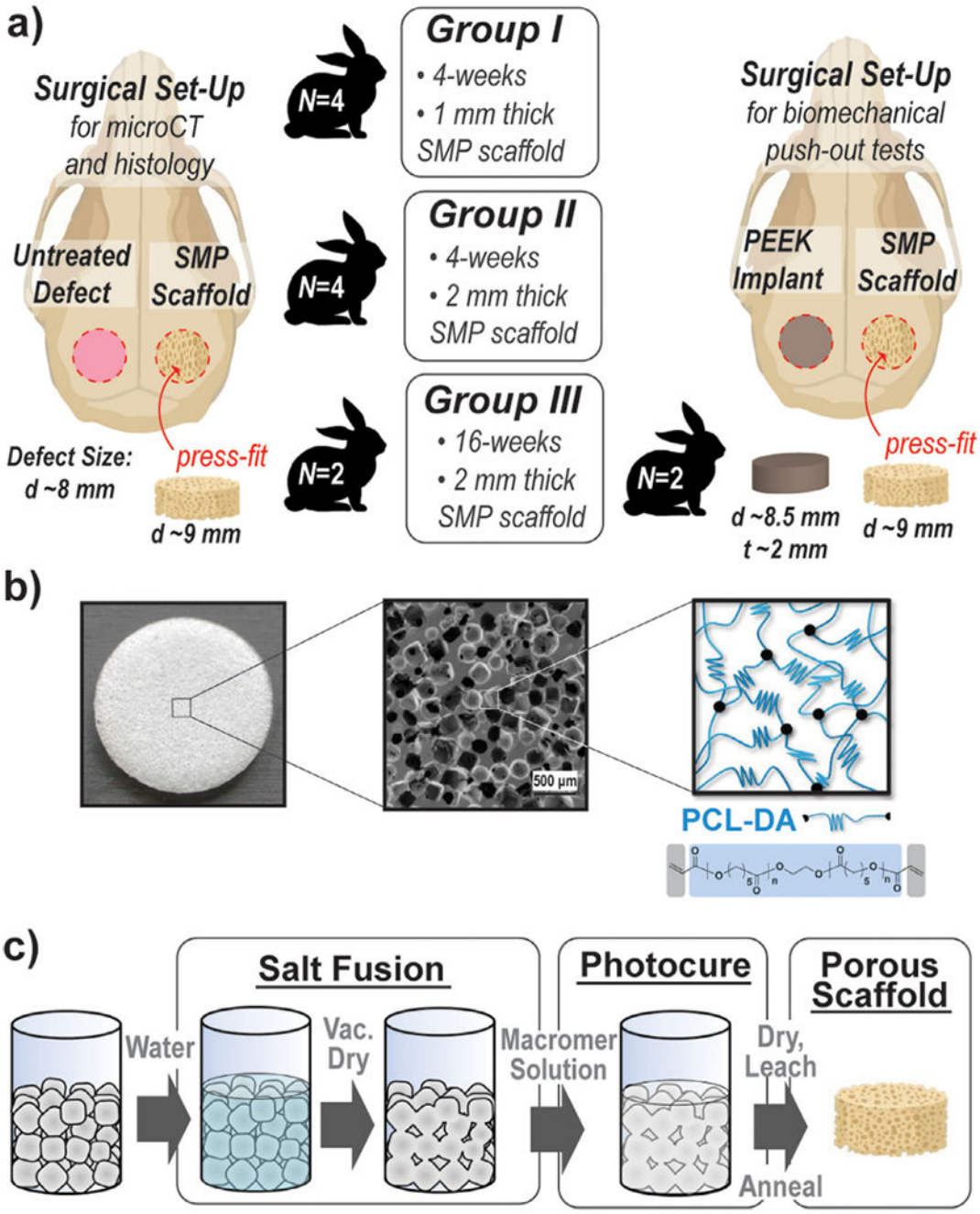

Fig. 1.

(a) An overview of the pilot studied performed using three groups of New Zealand white rabbits ($N = 4$ per group) with bilateral calvarial defects ($d = 8$ mm); (b) porous SMP scaffolds prepared from PCL-DA (M_n = 10k g/mol); (c) fabrication of SMP scaffolds via solvent casting particulate leaching (SCPL) with a fused salt template to afford interconnected pores [~220 µm pore diameter, ~70% porosity].

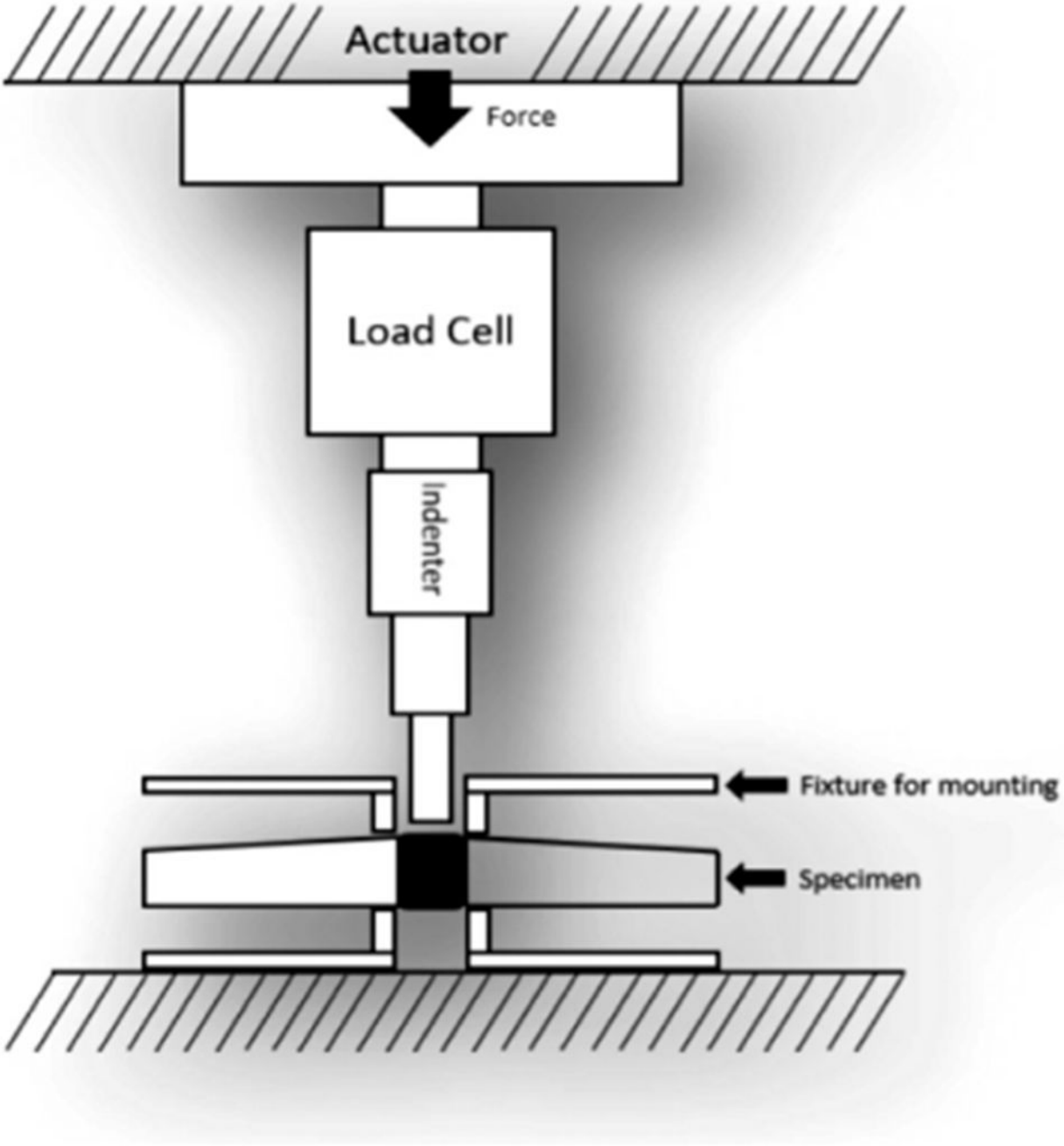

Fig. 2.
Schematic of custom biomechanical testing apparatus.

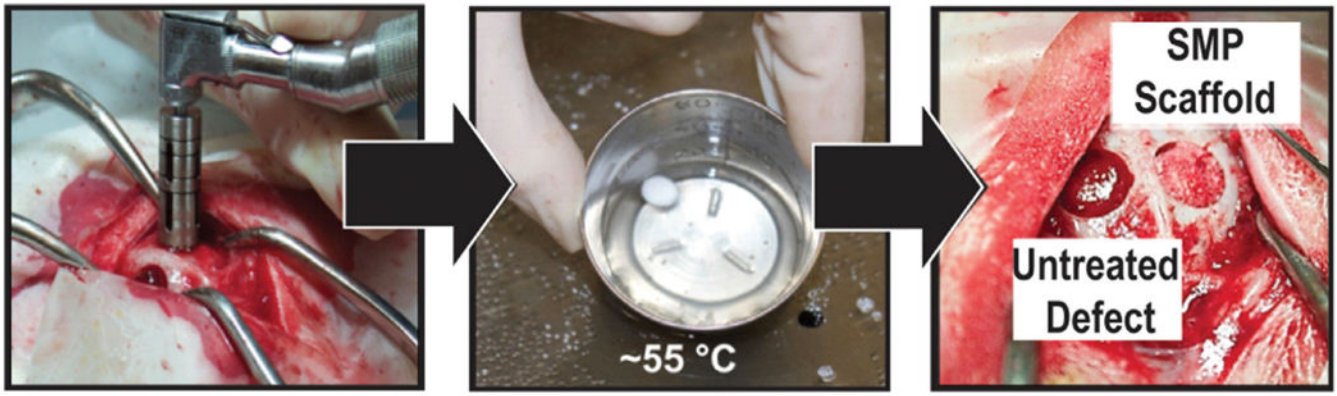

Fig. 3.
"Self-fitting" SMP scaffolds were readily implanted by briefly warming in saline (T ~55 °C) and then press-fitting into the calvarial defect.

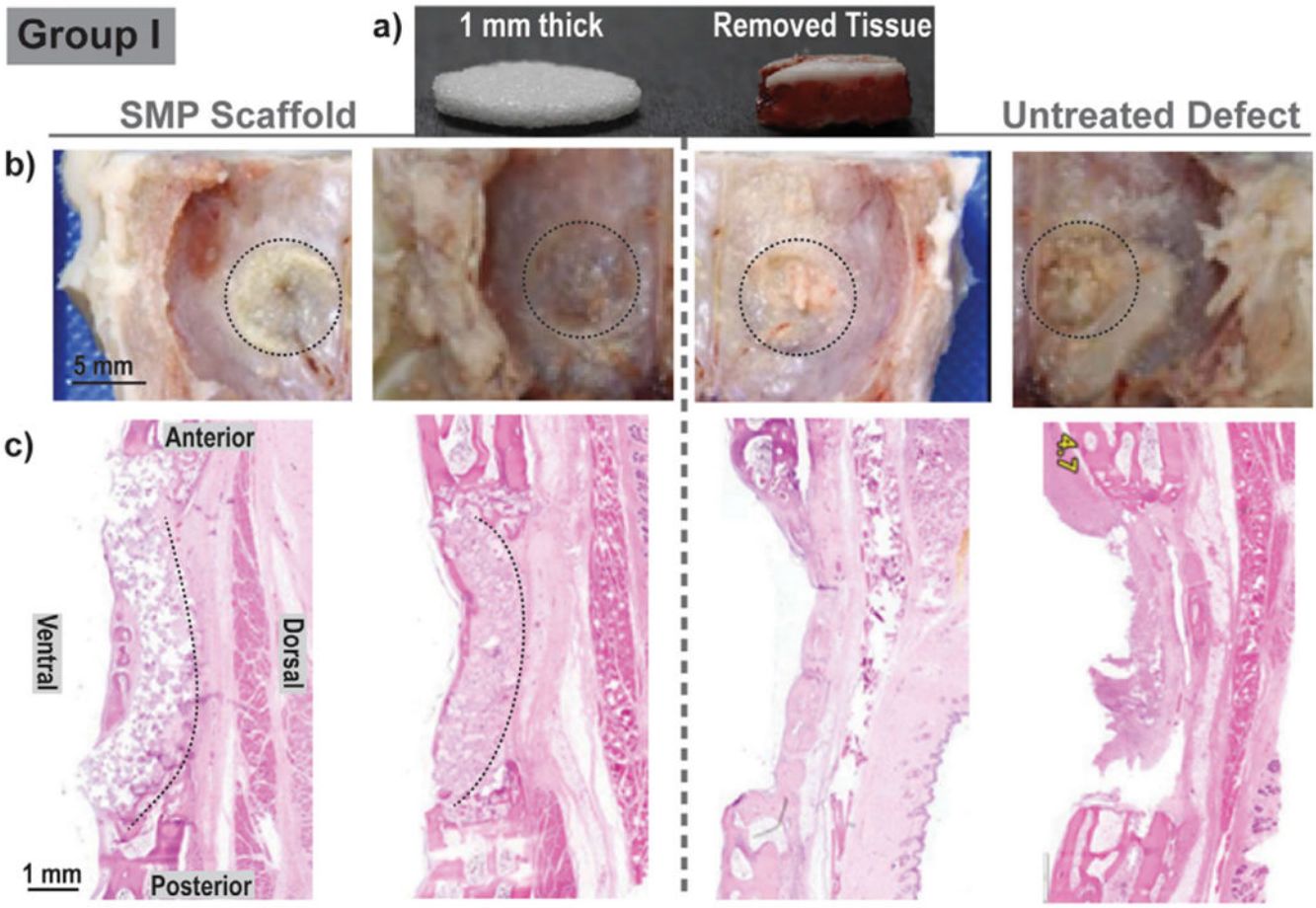

Fig. 4.

Group I: For each animal ($N = 4$), bilateral defects ($d = 8$ mm) were treated with a scaffold ($d = 9$ mm x $t = 1$ mm) [left], or remained untreated [right]; healing was assessed at 4 weeks. **(a)** The SMP scaffold was somewhat thinner versus the removed calvarial defect tissue; **(b)** Gross examination did not show appreciable difference between the defects treated with an SMP scaffold and untreated defects; **(c)** Histology (H&E staining) showed signs of SMP scaffold bowing, attributed to the thickness mismatch.

Notes: Two representative gross images and two representative histological images were selected. 'Black dashed lines' were used to outline the defect site in gross examination photos and to demonstrate scaffold positioning in histology sections.

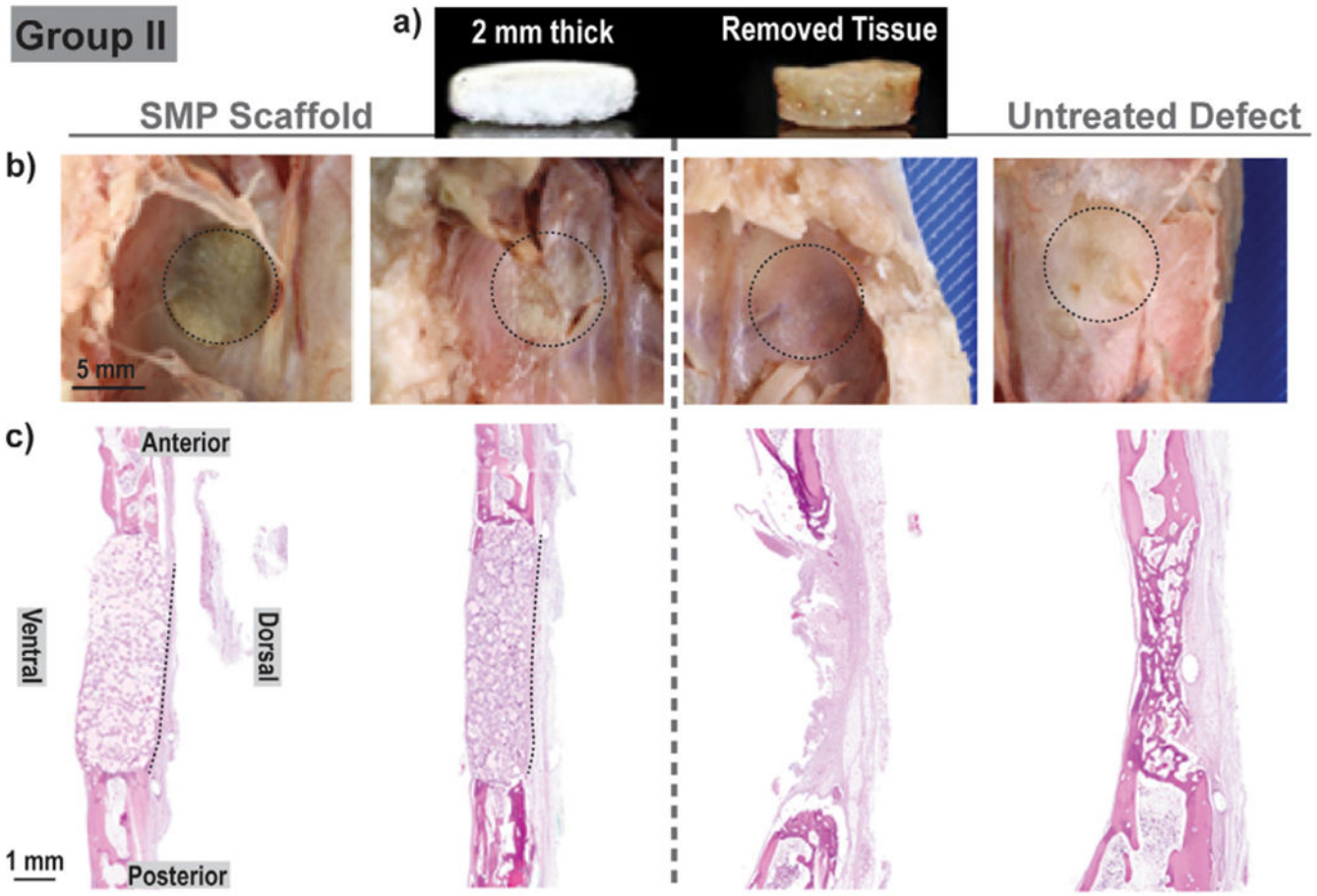

Fig. 5.

Group II: For each animal ($N = 4$), bilateral defects ($d = 8$ mm) were treated with a scaffold ($d = 9$ mm x $t = 2$ mm) [left], or remained untreated [right]; healing was assessed at 4 weeks. **(a)** SMP scaffold thickness was similar to the removed calvarial defect tissue; **(b)** Gross examination did not show appreciable difference between the defects treated with an SMP scaffold and untreated defects; **(c)** Histology (H&E staining) showed no signs of SMP scaffold bowing.

Notes: Two representative gross images and two representative histological images were selected. 'Black dashed lines' were used to outline the defect site in gross examination photos and to demonstrate scaffold positioning in histology sections.

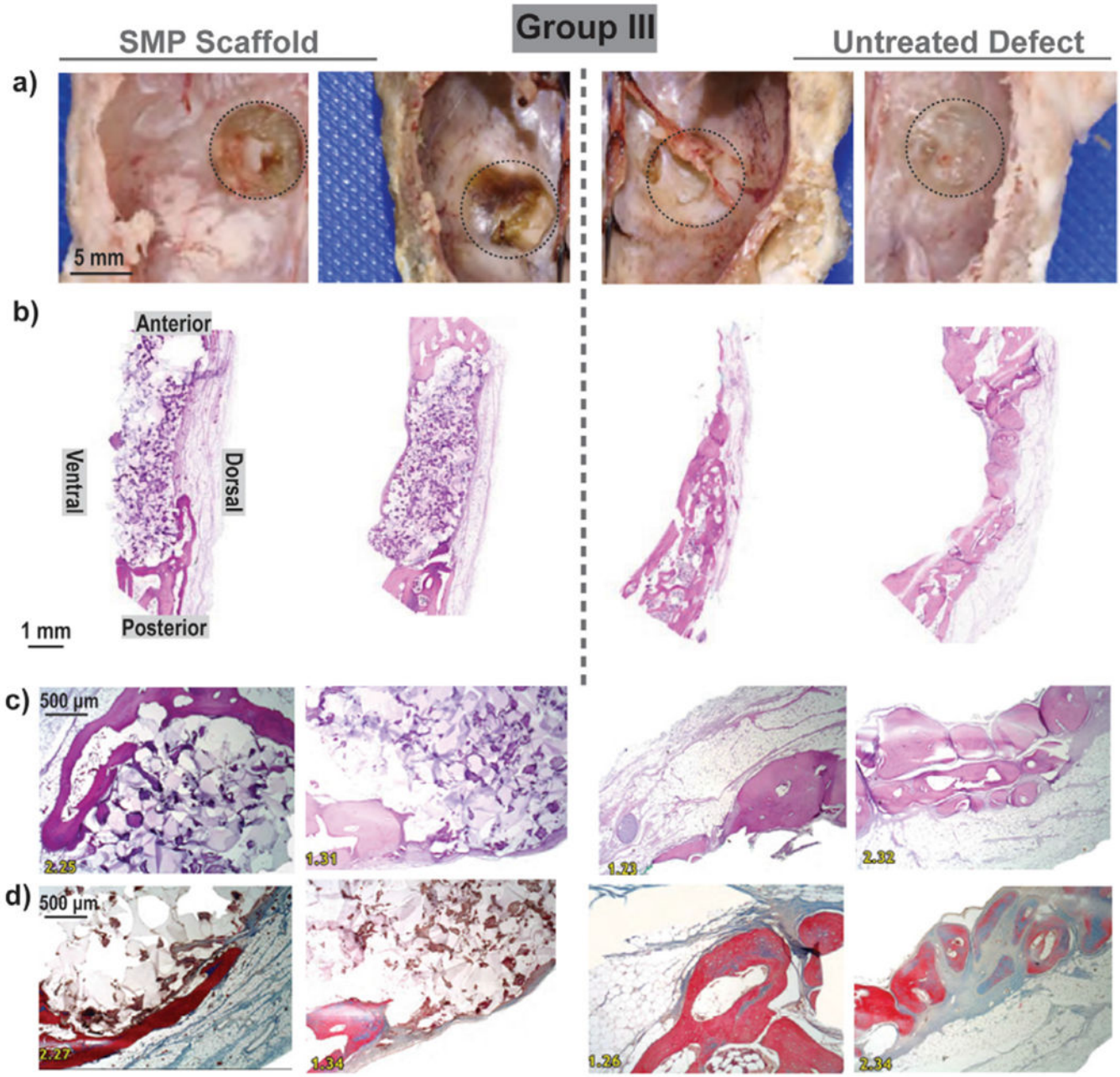

Fig. 6.

Group III: For each animal ($N = 2$), bilateral defects ($d = 8$ mm) were treated with a scaffold ($d = 9$ m x $t = 2$ mm) [left], or remained untreated [right]; healing was assessed at 16 weeks. **(a)** Gross examination showed evidence of scaffold persistence and slight bulging on ventral surface; **(b)** Low magnification histology (H&E staining) confirmed presence of SMPs with fibrous and bony tissue formation adjacent to the dorsal and ventral surfaces of the implants. Untreated defects contained fibrous tissue within the defect **(c)** H&E and **(d)** Trichrome staining high magnification histology confirmed biocompatibility as well as fibrous and bony ingrowth at the periphery.

Notes: Two representative gross images and two representative histological images were selected. ‘Black dashed lines’ were used to outline the defect site in gross examination photos and to demonstrate scaffold positioning in histology sections.

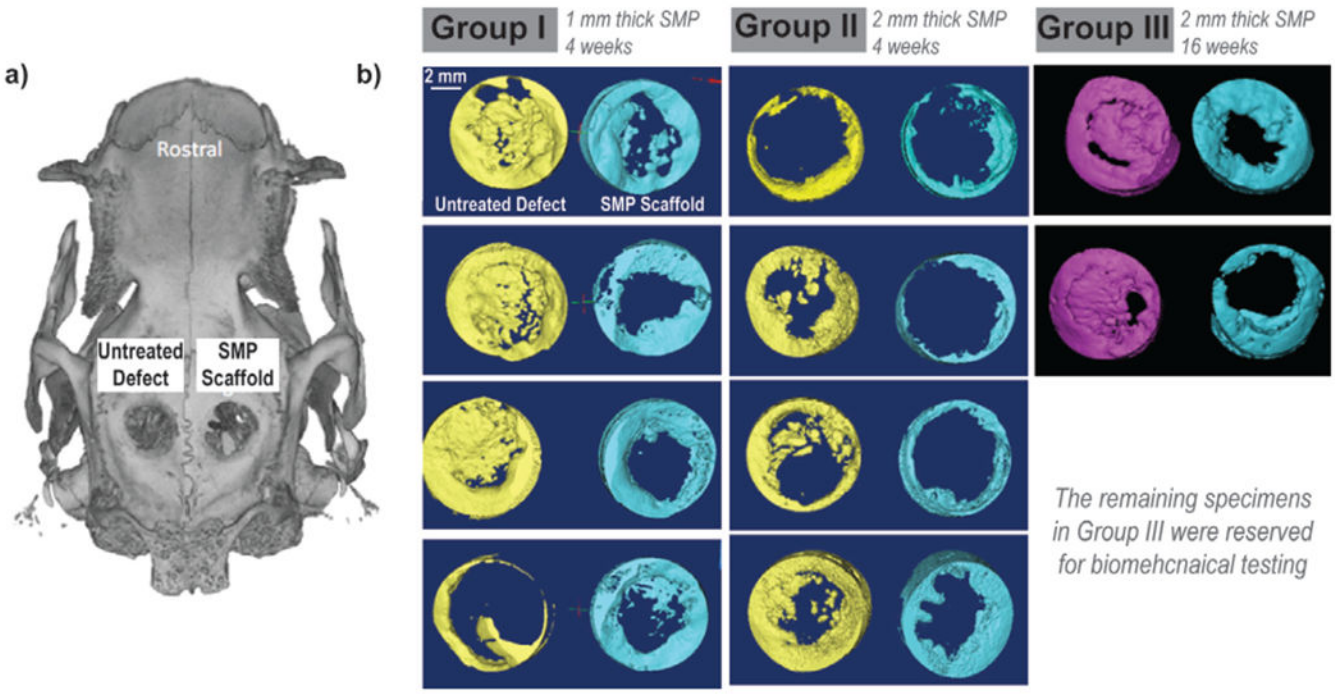

Fig. 7.

Micro-CT of Groups I, II, and III. **(a)** A representative micro-CT; **(b)** 3D reconstructions generated for all animals.

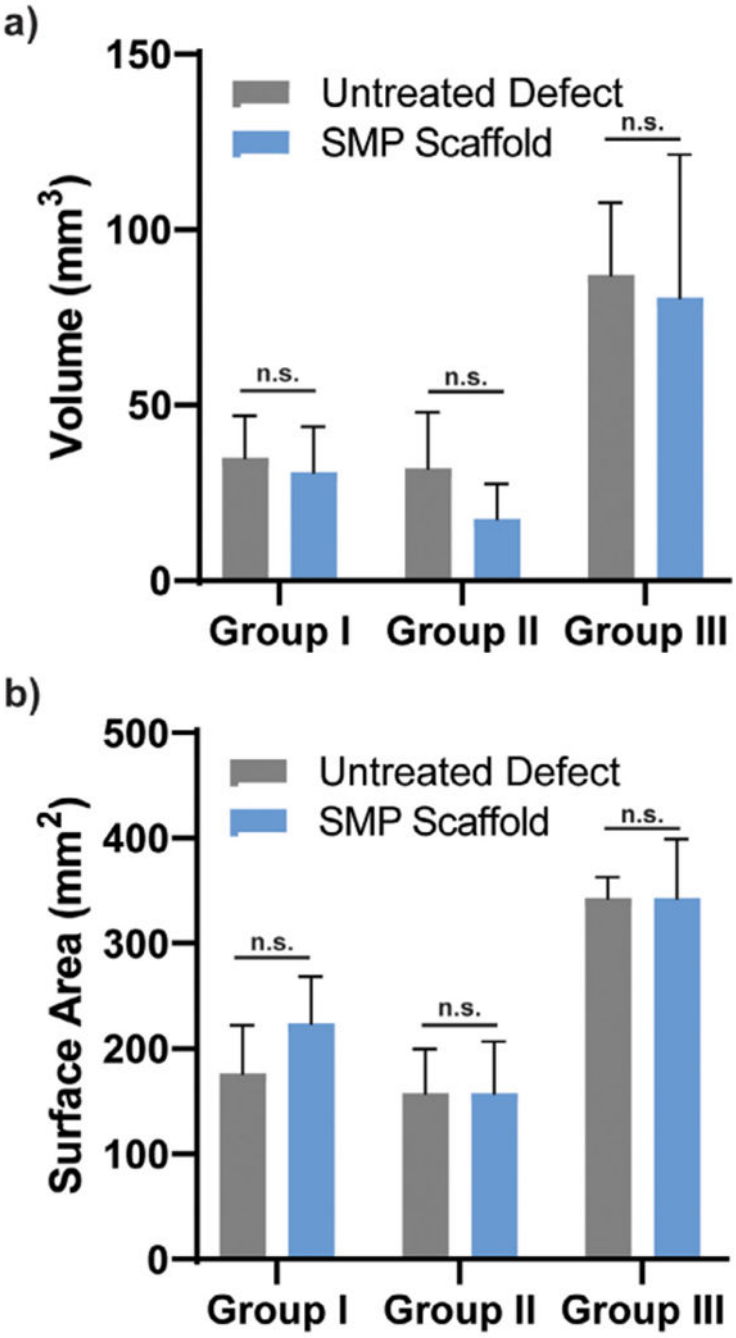

Fig. 8.

Overall bone quantification based on micro-CT reconstructions in terms of **(a)** volume and **(b)** surface area, *n.s.* indicates no statistical difference (*$p < 0.05$) compared to untreated defects within the same surgical group.

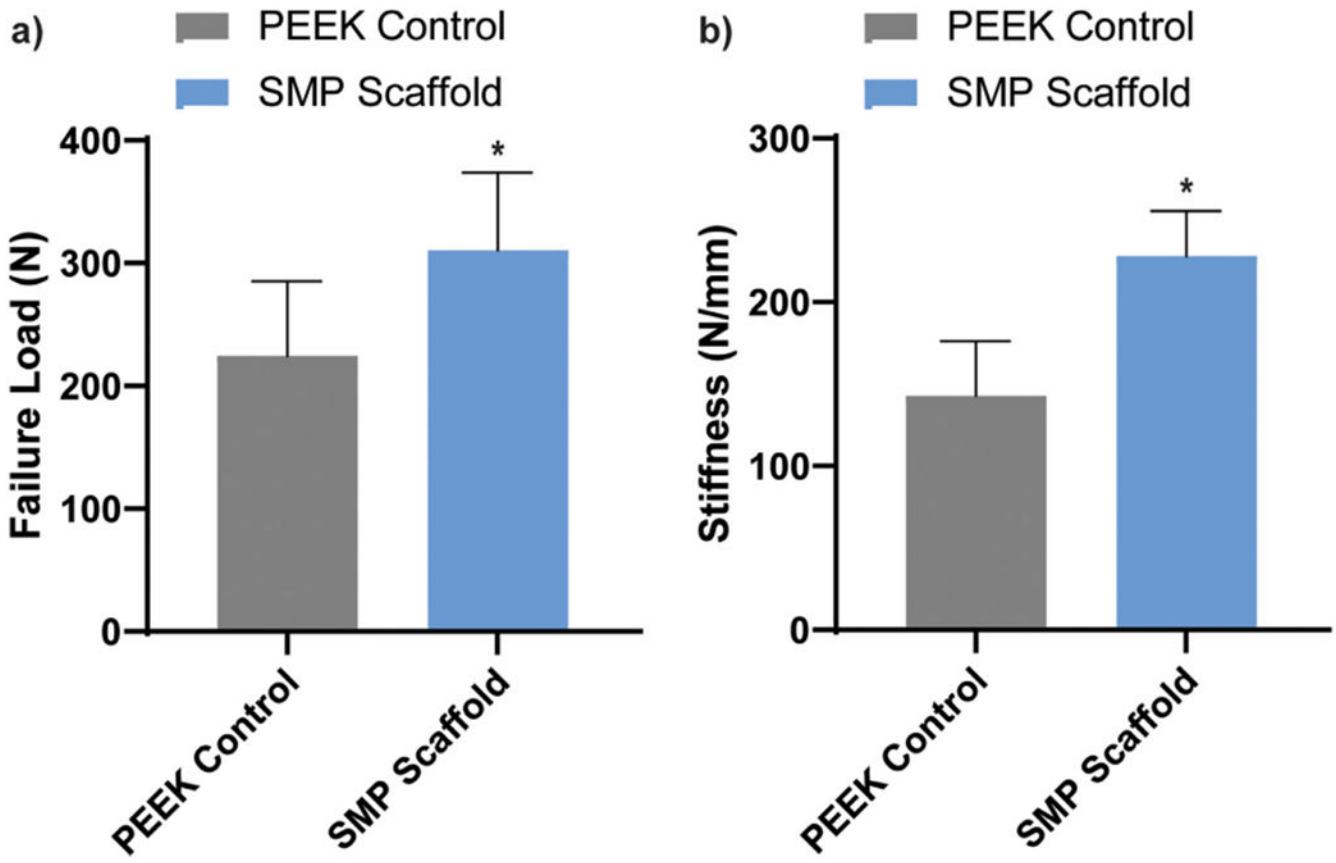

Fig. 9.

(a) Failure load and **(b)** stiffness determined via biomechanical push-out tests, $*p < 0.05$.

Table 1

Scaffold properties with and without sterilization (gamma irradiation).

Specimen	Ave. pore size (μm)	Porosity (%)	$T_{m,\ onset}$ (°C)	$T_{m,\ midpoint}$ (°C)	% cryst.	Modulus (MPa)	Strength (MPa)
Non-sterilized	226 ± 23	69.8 ± 0.8	51.8 ± 0.4	57.9 ± 0.5	62.1 ± 1.1	22.1 ± 4.2	25.8 ± 2.0
Sterilized	222 ± 25	70.5 ± 2.2	52.0 ± 0.6	58.0 ± 0.3	57.8 ± 3.0	18.0 ± 5.9	27.6 ± 6.4